Title
Probing Blue-Shifting Hydrogen Bonds with Adiabatic Energy Decomposition Analysis

Journal
The Journal of Physical Chemistry Letters, 10(14)

ISSN
1948-7185

Authors
Mao, Yuezhi
Head-Gordon, Martin

Publication Date
2019-07-18

DOI
10.1021/acs.jpclett.9b01203

Probing Blue-Shifting Hydrogen Bonds with Adiabatic Energy Decomposition Analysis

Yuezhi Mao[†] and Martin Head-Gordon[*,†,‡]

† *Kenneth S. Pitzer Center for Theoretical Chemistry, Department of Chemistry, University of California at Berkeley, Berkeley, CA 94720, USA*

‡ *Chemical Sciences Division, Lawrence Berkeley National Laboratory, Berkeley, CA 94720, USA*

E-mail: mhg@cchem.berkeley.edu

Abstract

The physical origin of blue-shifting hydrogen bonds remains a subject of debate although many plausible explanations have been proposed. Using a molecular property decomposition analysis based on absolutely localized molecular orbitals (ALMOs), we investigated several representative $F_3CH\cdots Y$ ($Y = H_2O$, NH_3, Cl^-) complexes. We reveal that features of a blue-shifting H-bond already appear on the frozen surface where polarization and charge-transfer (CT) are both "turned off", and that the final observed frequency shift depends on the strength of CT. Further decomposition of forces at the frozen level shows that Pauli repulsion is the only component that shortens the C–H bond when F_3CH and Y are close in contact, while both permanent electrostatics and dispersion tend to lengthen the bond. The interplay of these forces from the medium to long range is also discussed. Our analysis provides a complete

physical picture for shifting H-bonds and suggests two necessary conditions for their features to be observed at the equilibrium structure: (i) stronger Pauli repulsion than the combination of electrostatic and dispersion forces; (ii) relatively weak CT that is insufficient to compensate for the blue-shifting effect of the frozen interaction.

Table of Contents Graphic

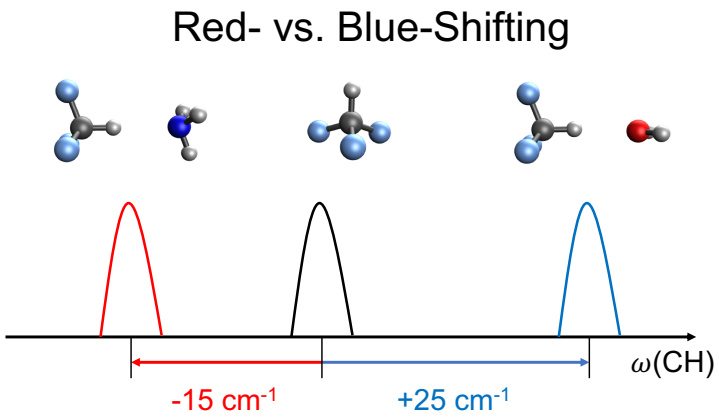

While a typical hydrogen-bonding complex X–H$\cdots$Y is associated with an increased X–H bond length and a red shift in XH stretch frequency relative to those in a free XH molecule,[1] there exist exceptions whose X–H bond is contracted and its stretch frequency blue-shifted. Those exceptional cases were referred to as "improper, blue-shifting" H-bonds by Hobza et al.[2,3] The blue-shifted XH stretch frequencies can be characterized experimentally,[4–10] and due to its apparent peculiarity, there has been a plethora of computational studies aiming to unravel the origin of blue-shifting H-bonds, but no consensus has been reached as the conclusion varies with the analysis tool employed and the interpretation of results. To list a few, the origin of bond contraction and frequency blue-shifting has been attributed to dispersion interactions,[4,11,12] charge transfer (CT),[2,3,6] electrostatics,[13–17] Pauli repulsion,[18–21] electron density redistribution/polarization,[10,22–24] etc. Even today, the physical origin of blue-shifting H-bonds still remains a subject of debate.

Using an analysis based on block-localized wavefunctions (BLW),[25–27] Mo and co-workers obtained optimal structures and harmonic frequencies of a series of $F_3CH\cdots Y$ (Y = NH_3, H_2O, or HF) complexes with CT being forbidden or "quenched".[17] Their results indicate that CT causes bond lengthening and frequency red-shifting so it is *not* the reason for blue-shifting H-bonds. Furthermore, these authors identified that shortening of the C–H bond is a long-range phenomenon, and therefore they attributed this phenomenon to permanent electrostatics as it is the only non-trivial component at long range. In a follow-up study,[28] Wang et al. revealed that the frozen (FRZ) component of energy decomposition analysis (EDA) in fact does prefer a shortened C–H bond while both polarization (POL) and charge-transfer (CT) prefer a lengthened one. This identification was achieved by evaluating the derivative of each energy component with respect to the change in C–H bond length (Δr_{CH}). However this analysis might be affected by its use of fully relaxed geometries, at which the FRZ component is inclined to exert a strongly repulsive force due to the close intermolecular contact driven by POL and CT (see the discussion in ref. 29).

In previous work, we reported nuclear gradient for the FRZ intermediate state within the framework of the absolutely localized molecular orbital (ALMO)-EDA,[30,31] enabling a decomposition of molecular property shifts upon intermolecular binding into FRZ, POL, and CT contributions.[29] While the CT-forbidden (yet polarized) state in ALMO-EDA is essentially the same as that in BLW-EDA, additional insights can be gained by examining the structural and vibrational properties calculated on the FRZ surface, as the latter excludes all orbital relaxation effects. This scheme is referred to as the *adiabatic* ALMO-EDA (as the complex geometry is relaxed on each intermediate surface), and it has been employed to investigate the features of hydrogen and halogen bonds.[29,32,33] In this work, we use it to explore H-bonding complexes with the fluoroform molecule as the proton donor, which can be denoted as $F_3CH\cdots Y$. Table 1 shows the results for Y = H_2O, NH_3, and Cl^-, among which only the complex with H_2O has a shortened and blue-shifted C–H bond at the fully relaxed structure. However, on the FRZ surface, the C–H bonds in all three complexes are considerably shortened and blue-shifted, while POL and CT only contribute to bond lengthening and frequency red-shifting. The red-shifting effect of POL is remarkable for the complex with Cl^- yet minimal for the neutral complexes, and it is insufficient to offset the blue-shifting effect of FRZ. The final shift in C–H stretch frequency depends on the strength of CT, which, as shown in our previous studies,[29,32,34] is primarily responsible for the red shifts in conventional H-bonds. The requirement for relatively weak CT (also known as hyperconjugation) by an blue-shifting H-bond was also specifically noted in several previous studies despite their attribution of the blue-shifting feature to other physical origins.[17,23,28]

Results in Table 1 clearly demonstrate that the shortening and blue-shifting of C–H is an effect of FRZ interaction. This also holds for Si- and P-containing blue-shifting H-bonds as shown (Table S1 in the Supporting Information), indicating that the key role of FRZ is not specific to F_3CH complexes. As shown in our previous work, the FRZ term can be further separated into contributions from permanent electrostatics (ELEC), Pauli repulsion

Table 1: Adiabatic ALMO-EDA results for $F_3CH\cdots Y$ (Y = H_2O, NH_3, and Cl^-) complexes, including C–H bond lengths (Å) and vibrational frequencies (cm^{-1}) calculated on the frozen (FRZ), polarized (POL), and fully relaxed (FULL) surfaces as well as the associated energy lowerings (in kJ/mol). The shifts in molecular properties are calculated relative to the results of fully relaxed CF_3H: r(C–H) = 1.0917 Å, ω(C–H) = 3151 cm^{-1}.

	$F_3CH\cdots H_2O$			$F_3CH\cdots NH_3$			$F_3CH\cdots Cl^-$		
	FRZ	POL	FULL	FRZ	POL	FULL	FRZ	POL	FULL
r(C–H)	1.0894	1.0896	1.0906	1.0893	1.0898	1.0928	1.0860	1.0895	1.1030
Δr	-0.0023	-0.0021	-0.0011	-0.0024	-0.0019	0.0011	-0.0057	-0.0022	0.0113
ω(C–H)	3198	3195	3176	3198	3190	3136	3252	3208	2990
$\Delta\omega$	47	44	25	47	39	-15	101	57	-161
ΔE	-10.95	-1.84	-1.95	-12.95	-2.41	-3.38	-41.27	-12.24	-12.57

(PAULI), and dispersion (DISP).[35] To identify the component that is responsible for bond shortening (which almost always accompanies frequency blue-shifting), we decomposed the intermolecular forces exerted on the H atom along the C–H bond direction at the optimal FRZ structure of each complex. The results (Fig. 1) indicate that Pauli repulsion is the only component that favors a shortened C–H bond, while both ELEC and DISP tend to stretch the bond further. The opposite effects of PAULI and DISP are somewhat consistent with chemical intuition, as the closer contact between H and Y makes the former more unfavorable while the latter more attractive. However, the effect of ELEC differs from what one would infer from the "long-range" character of the bond-shortening phenomenon,[17,28] or from the negative dipole derivative of CF_3H with respect to r_{CH}.[13,15] Among the literature on blue-shifting H-bonds, our finding is most consistent with the conclusions reached independently by Li et al.[19] and Hermansson,[20] who found that ELEC alone is unable to cause C–H blue-shifting (by using a point-charge model to replace Y) and suggested the necessity of a repulsive force.

As Pauli repulsion decays faster than ELEC and DISP, one may expect an "inverted regime" to appear at a longer distance where the overall effect of FRZ interaction becomes bond-lengthening. To verify this, we probe the change in optimal C–H bond length with varying C$\cdots$O (N, Cl) distances (constrained in geometry optimization) for the three com-

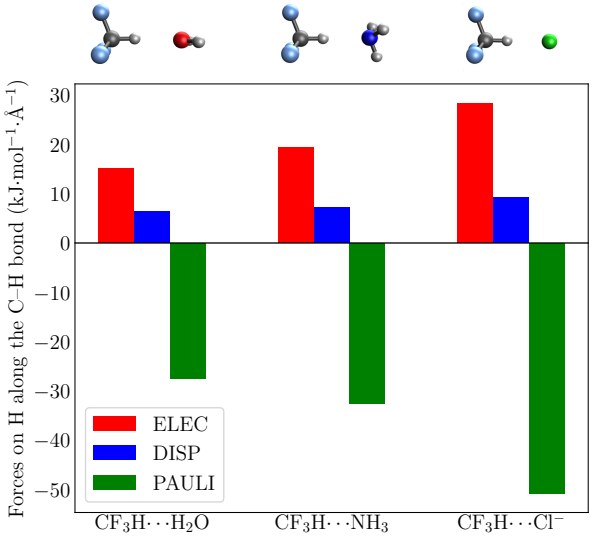

Figure 1: Decomposition of intermolecular forces on the H atom in CF_3H (along the C–H bond) at the optimal structures of $F_3CH\cdots Y$ ($Y = H_2O$, NH_3, and Cl^-) on the frozen surface. Positive forces stretch the bond while negative forces compress it. Note that the plotted three components do not add up to the total force for the FRZ state (which is zero for these optimized structures) as the latter also includes an intramolecular contribution from monomer geometry distortion.

plexes. The results for H_2O [Fig. 2(a)] and NH_3 complexes [Fig. 2(c)] resemble each other on the FRZ surface, i.e., a transition from bond shortening to lengthening *does* occur after going beyond the equilibrium $C\cdots O/C\cdots N$ distance (denoted by red vertical dashed lines). On the POL and FULL surfaces, the variation of C–H bond length with respect to intermolecular distance shows similar behavior, although the bond shortening at close distances is less significant and the transition to lengthening occurs at smaller distances. At fully relaxed structures (blue vertical dashed lines), the C–H bond is still shortened in the complex with H_2O (associated with frequency blue-shifting) but already lengthened in $F_3CH\cdots NH_3$ (associated with red-shifting), resulting from the stronger CT effect in the latter complex.

We then decomposed the intermolecular FRZ forces exerted on the H atom in F_3CH along the C–H bond [Figs. 2(b) and 2(d)]. Across the entire plotting range (3 Å $< R(C\cdots Y) <$ 5 Å), the effect of ELEC, DISP, and PAULI forces on the C–H bond length is consistent with that as revealed in Fig. 1. The PAULI force is of larger magnitude than the other two

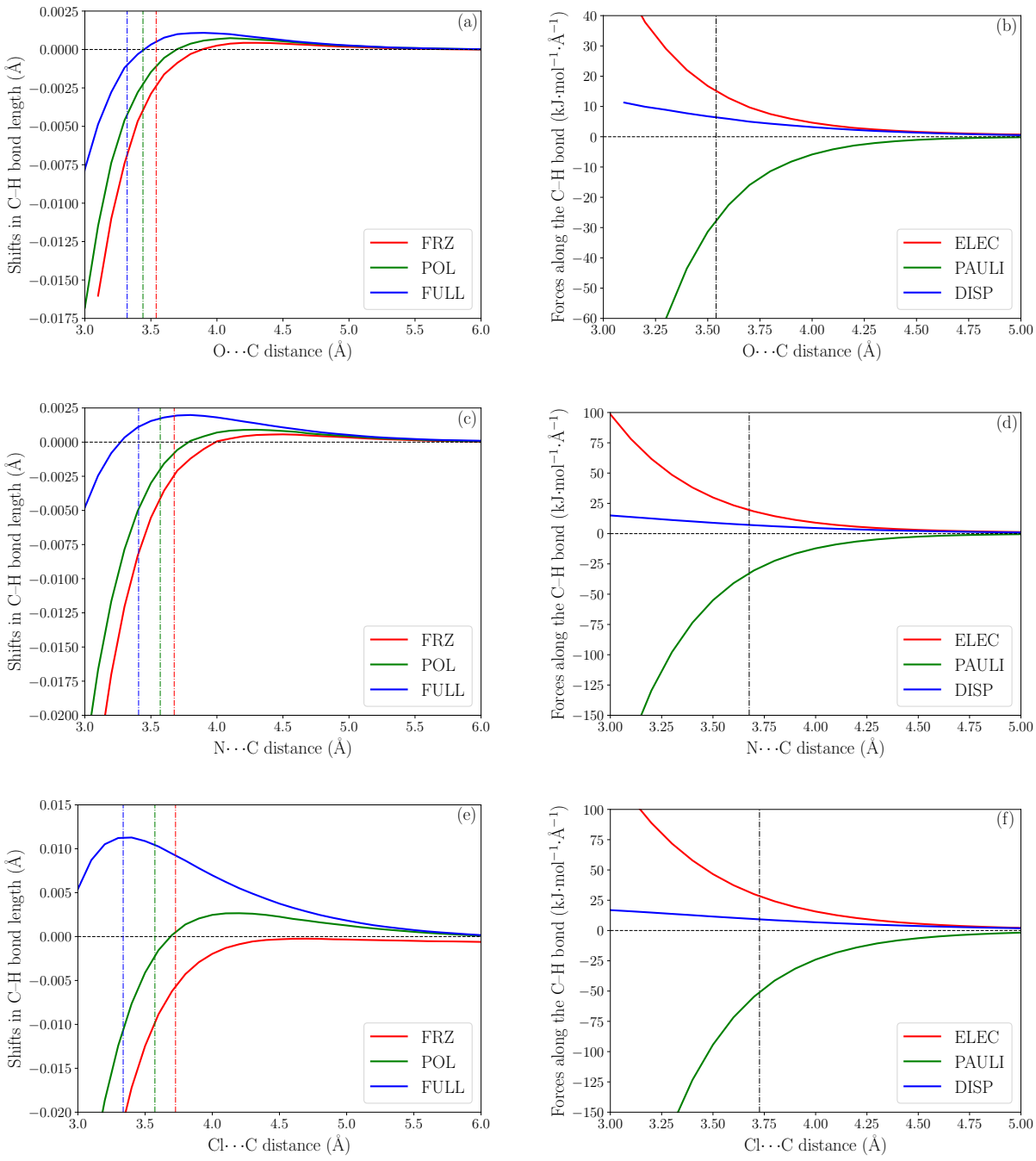

Figure 2: Left panels: variations of the optimal C–H bond length in $F_3CH{\cdot\cdot}H_2O$ (a), NH_3 (c), Cl^- (e) with the C··Y distance (calculated on frozen, polarized, and fully relaxed surfaces); right panels: decomposition of intermolecular forces exerted by H_2O (b), NH_3 (e), and Cl^- (f) on the H atom (along the C–H bond) calculated with structures optimized on the FRZ surface.

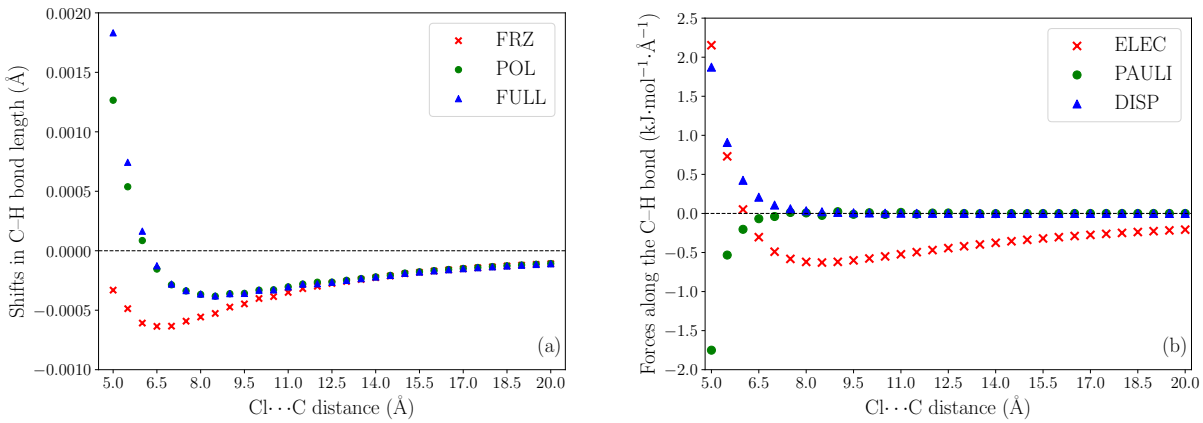

Figure 3: Long-range scan results for the $F_3CH\cdots Cl^-$ complex: (a) variation of optimal C–H bond length calculated on the FRZ, POL, and FULL surfaces; (b) decomposition of FRZ forces due to Cl^- exerted on the H atom along the C–H bond.

bond-lengthening components around the equilibrium distance, resulting in bond shortening in this range. Nonetheless, with the increase of intermolecular separation, the magnitude of the sum of ELEC and DISP forces eventually surpasses that of PAULI, resulting in a reversed change in C–H bond length (elongation) on the FRZ surface.

The variation of optimal C–H bond length shows somewhat different behavior for the $F_3CH\cdots Cl^-$ complex [Fig 2(e)]. On the FULL surface, the bond is much more significantly elongated (about 10 times compared to the amount of lengthening in $F_3CH{\cdot\cdot}NH_3$) as a result of the stronger CT effect. On the other hand, the curve corresponding to the FRZ surface remains negative for the entire range, and one can see a shallow dip (corresponding to more significant shortening) after $R(Cl\cdots C)$ goes beyond 4.5 Å. The changes in the optimal bond length at long range are more clearly demonstrated in Fig. 3(a): on the FRZ surface, the bond length reaches a minimum at around 6.5 Å and then goes back gradually towards the free monomer bond length; the results on POL and FULL surfaces track each other closely after 6 Å, and the minimum is located at a longer distance compared to that on the FRZ surface. The force decomposition performed on the FRZ surface [Fig. 3(b)] suggests that

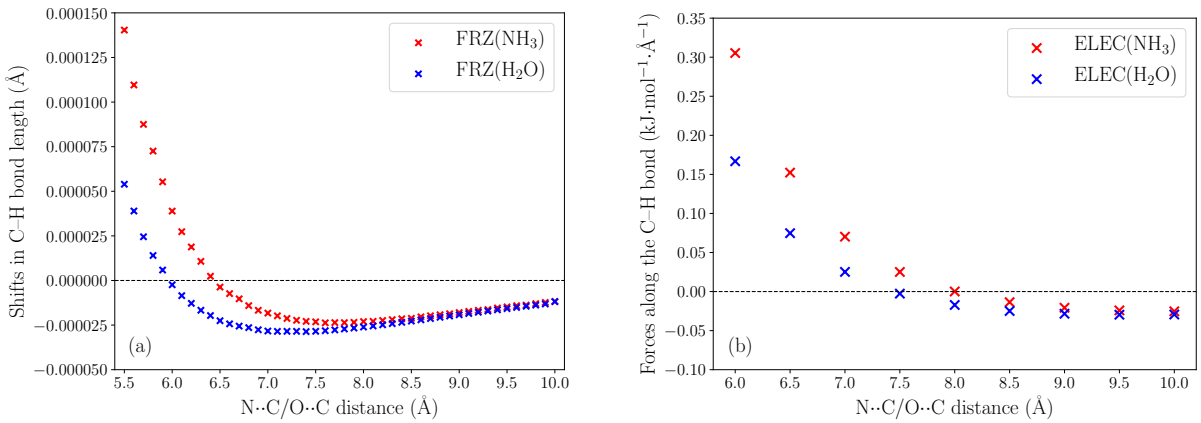

Figure 4: (a) Variation of optimal C–H bond length in $F_3CH\cdots H_2O$, NH_3 complexes on the FRZ surface; (b) the permanent electrostatic force exerted on the H atom (along the C–H bond). The PAULI and DISP forces vary similarly to their behavior in Fig. 3(b) and are not plotted here. The complete results are available in Fig. S2 of the Supporting Information.

the characteristic change of the ELEC component should be related to the dip in optimal C–H bond length: when the $Cl\cdots C$ distance is greater than 6 Å, ELEC turns into a bond-shortening force instead and then slowly decays to zero. The decrease in optimal C–H bond length at long range takes place for $F_3CH{\cdot\cdot}H_2O$ and $F_3CH\cdots NH_3$ as well [Fig. 4(a)], although the amount of shortening is over one order of magnitude smaller. The ELEC force changes its character (from bond-lengthening to shortening) roughly at 7.5 Å and 8.0 Å, respectively [Fig. 4(b)]. Note that for all three complexes, the decrease in C–H bond length is not synchronized with the characteristic change in the ELEC force. Instead, the former occurs at a shorter intermolecular distance, as a result of the interplay with forces arising from monomer geometry distortion.

The transition in character of the ELEC force suggests the existence of two competing effects, whose nature is elucidated in Fig. 5: (i) Based on ChElpG charges, a longer C–H bond renders the H atom more positive and in closer contact with the electronegative species Y, which enhances the favorable electrostatic interaction; (ii) the permanent dipole of F_3CH increases when the C–H bond is shortened, rendering a shortened C–H bond more

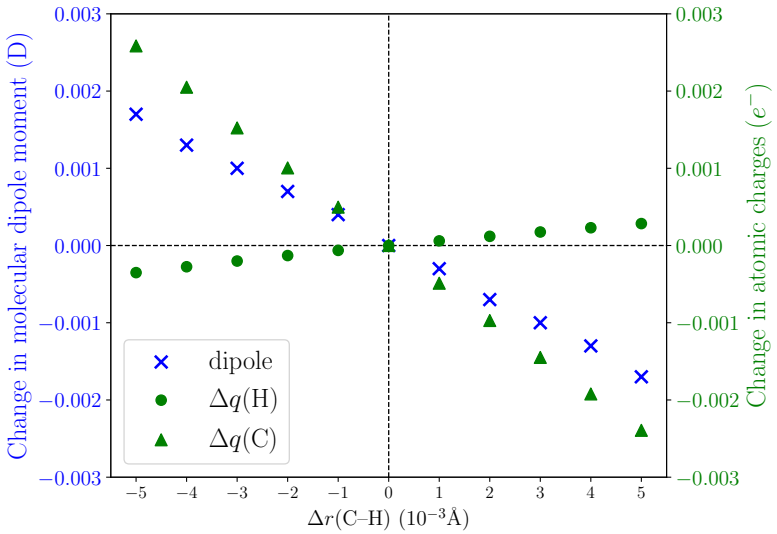

Figure 5: Changes in dipole moment of the isolated F_3CH molecule (blue) and ChElpG charges[36] on C and H atoms (green) with respect to variation of C–H bond length. The monomer geometry is relaxed at each given C–H bond length (constrained in optimization).

favorable from the perspective of a multipole interaction. As shown in Fig. 5, more electron population is depleted from the C atom than that gained on H when $\Delta r < 0$, making the F end more negative. One can thus infer that the shift in charge distribution govern the change in F_3CH's dipole moment. Using an abstract model system as depicted in Fig. 6, it can be proven that there exists a critical distance R_c. When $R < R_c$, effect (i) is dominant and a lengthened C–H bond is more favorable by ELEC; when $R > R_c$, effect (ii) plays the more significant role and a shortened C–H bond is preferred instead. The mathematical details for this qualitative analysis are available in Sec. S1 of the Supporting Information.

It should be noted that the negative dipole derivative with respect to r_{CH} was reported and designated as the cause of C–H bond shortening and blue-shifting by others.[13,15] The bond-shortening behavior in the long range was also regarded as the evidence for ELEC being the origin of blue-shifting H-bonds.[17,28] The analysis performed in our work, however, clearly demonstrates that electrostatic force alone is unable to induce the C–H bond shortening and frequency blue-shifting at the equilibrium structure, where ELEC actually

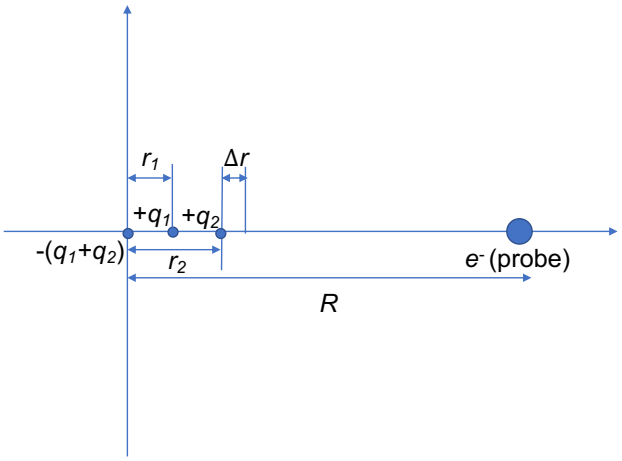

Figure 6: Model system for qualitatively illustrating the distance-dependence of the permanent electrostatic interaction between F_3CH (abstracted as three point charges at the position of the center of three F atoms, the C atom, and the H atom, respectively) and an electronegative species (abstracted as a probe negative charge whose distance from the origin is R). The small displacement of the H atom is denoted as Δr. Based on Fig. 5, we assume that the charge on C(H) linearly decreases(increases) with respect to Δr: $q_1' = q_1 - k_1\Delta r$, $q_2' = q_2 + k_2\Delta r$ $(k_1 > k_2)$.

has an opposite effect. Our findings, on the other hand, are in better agreement with the conclusion reached by Hermansson that the negative dipole derivative is "a necessary but not sufficient" condition for blue-shifting,[20] because it prevents the X–H bond from being substantially lengthened before the onset of Pauli repulsion. In fact, the involvement of long-range electrostatics is *not* necessary for the change in bond length around equilibrium distance, and blue-shifting H-bonds with X = O or N whose dipole derivative with respect to r_{XH} is positive have also been discovered and rationalized in computational studies.[19,23] Fig. 7 shows the variation in optimal C–H bond length on the FRZ surface when F_3CH interacts with rare gas atoms (Ne, Ar, and Kr), for which the contribution from long-range ELEC is zero by definition as these atoms have no permanent multipole moments. The curve corresponding to the F_3CH complex with Ne shows behavior similar to those for H_2O and NH_3 [Figs. 2(a) and 2(c)], despite its much less pronounced bond elongation beyond equilibrium. Heavier rare gas atoms result in more significant bond shortening in the short range, as they exert stronger Pauli repulsion when placed at the same distance from F_3CH.

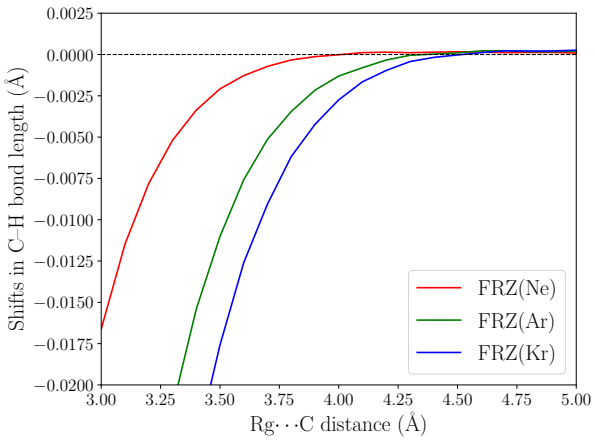

Figure 7: Variation of optimal C–H bond lengths calculated on the FRZ surface of $F_3CH{\cdot\cdot}Rg$ (Rg = Ne, Ar, Kr) complexes.

In summary, we investigated the physical origin of blue-shifting H-bonds formed by the CF_3H molecule using recently developed analysis tools based on ALMOs. It was found that C–H bond shortening and frequency blue-shifting can take place when POL and CT are both absent. Further analysis shows that the cause of bond shortening can be almost fully interpreted as the "mechanical compression" exerted on the H atom by the proton acceptor Y, which stems from intermolecular Pauli repulsion. Permanent electrostatics, on the other hand, is only capable of shortening the C–H bond minimally at long range, and it turns into a bond-lengthening force at smaller intermolecular separation. This nuanced behavior of electrostatic force was rationalized using a model system abstracted from the $F_3CH{\cdot\cdot}Y$ complexes. In addition to Pauli repulsion, relatively little CT is also required for the bond shortening and frequency blue-shifting result to hold, as CT always leads to red-shifting. Our analysis appears to fully unravel the underlying physical picture that gives rise to blue-shifting H-bonds, and we expect that the same tools can be applied to elucidate other intriguing changes in structural and spectroscopic observables arising from intermolecular interactions.

Computational Methods

All calculations were performed with the Q-Chem 5.1 software package.[37] The adiabatic EDA calculations (geometry optimizations and harmonic frequency analysis) were performed with the ωB97X-V functional[38] and the def2-TZVPPD[39] basis set. Extensive benchmarking[40,41] has established ωB97X-V as one of the most accurate density functionals for intermolecular interaction energies. In addition, we performed the adiabatic EDA involved in Table 1 as well as the long-range bond length analysis [Figs. 3(a) and 4(a)] with a different level of theory [B3LYP[42] with a Becke-Johnson damped D3 correction[43] and the 6-311++G(3df,3pd) basis set[44,45]] and confirmed that the same qualitative trends can be reproduced (see Table S2 and Fig. S3 in Supporting Information). The geometry optimizations were performed until the maximum component of the gradient is smaller than 2.0×10^{-6} a.u. and the energy change from the previous step is smaller than 1.0×10^{-7} a.u. For numerical integrations involved in DFT calculations, we use a (99, 590) grid (99 radial shells with 590 Lebedev points in each) for the exchange-correlation functional and SG-1[46] for the VV10[47] dispersion correction. The forces arising from frozen interaction components were calculated using a five-point stencil (five vertical EDA calculations with varying C–H bond lengths). The decomposition of the frozen term follows the scheme introduced in ref. 48, which employs the "quasiclassical" definition of permanent electrostatics (Coulomb interaction between charge distributions of isolated fragments).

Associated Contents

Supporting Information: qualitative analysis of the two features of the electrostatic interaction based on a simple model system; adiabatic EDA results for Si- and P-containing blue-shifting H-bonds; adiabatic EDA results (similar to Table 1) and plots for the variation of optimal C–H bond length in the long range [similar to Figs. 3(a) and 4(a)] for $F_3CH\cdots Y$

($Y = H_2O$, NH_3, and Cl^-) calculated at the B3LYP-D3(BJ)/6-311++G(3df,3pd) level of theory; long-range force decomposition results on the FRZ surface for $F_3CH\cdots H_2O$ and $F_3CH\cdots H_2O$ (PDF); equilibrium geometry of the CF_3H monomer and complex geometries optimized at the FRZ, POL, and FULL levels of theory (fully relaxed and with $C\cdots Y$ distance constrained) (ZIP).

Acknowledgments

This work was supported by Grant CHE-1665315 from the U.S. National Science Foundation (NSF).

References

(1) Arunan, E.; Desiraju, G. R.; Klein, R. A.; Sadlej, J.; Scheiner, S.; Alkorta, I.; Clary, D. C.; Crabtree, R. H.; Dannenberg, J. J.; Hobza, P.; Kjaergaard, H. G.; Legon, A. C.; Mennucci, B.; Nesbitt, D. J. Definition of the hydrogen bond (IUPAC Recommendations 2011). *Pure Appl. Chem.* **2011**, *83*, 1637–1641.

(2) Hobza, P.; Havlas, Z. Blue-shifting hydrogen bonds. *Chem. Rev.* **2000**, *100*, 4253–4264.

(3) Hobza, P.; Havlas, Z. Improper, blue-shifting hydrogen bond. *Theo. Chem. Acc.* **2002**, *108*, 325–334.

(4) Hobza, P.; Špirko, V.; Havlas, Z.; Buchhold, K.; Reimann, B.; Barth, H.-D.; Brutschy, B. Anti-hydrogen bond between chloroform and fluorobenzene. *Chem. Phys. Lett.* **1999**, *299*, 180–186.

(5) Reimann, B.; Buchhold, K.; Vaupel, S.; Brutschy, B.; Havlas, Z.; Špirko, V.; Hobza, P. Improper, blue-shifting hydrogen bond between fluorobenzene and fluoroform. *J. Phys. Chem. A* **2001**, *105*, 5560–5566.

(6) van der Veken, B. J.; Herrebout, W. A.; Szostak, R.; Shchepkin, D. N.; Havlas, Z.; Hobza, P. The nature of improper, blue-shifting hydrogen bonding verified experimentally. *J. Am. Chem. Soc.* **2001**, *123*, 12290–12293.

(7) Yu, Y.; Fan, W.; Wang, Y.; Zhou, X.; Sun, J.; Liu, S. C–H··· O Interaction in Methanol–Water Solution Revealed from Raman Spectroscopy and Theoretical Calculations. *J. Phys. Chem. B* **2017**, *121*, 8179–8187.

(8) Sosulin, I. S.; Shiryaeva, E. S.; Tyurin, D. A.; Feldman, V. I. Matrix Isolation and Ab Initio Study on the CHF3··· CO Complex. *J. Phys. Chem. A* **2018**, *122*, 4042–4047.

(9) Behera, B.; Das, P. K. Blue-and Red-Shifting Hydrogen Bonding: A Gas Phase FTIR and Ab Initio Study of RRCO··· $DCCl_3$ and RRS··· $DCCl_3$ Complexes. *J. Phys. Chem. A* **2018**, *122*, 4481–4489.

(10) Behera, B.; Das, P. K. Blue-Shifted Hydrogen Bonding in the Gas Phase $CH/D_3CN\cdots HCCl_3$ Complexes. *J. Phys. Chem. A* **2019**, *123*, 1830–1839.

(11) Hobza, P.; Špirko, V.; Selzle, H. L.; Schlag, E. W. Anti-hydrogen bond in the benzene dimer and other carbon proton donor complexes. *J. Phys. Chem. A* **1998**, *102*, 2501–2504.

(12) Zierkiewicz, W.; Jurečka, P.; Hobza, P. On Differences between Hydrogen Bonding and Improper Blue-Shifting Hydrogen Bonding. *ChemPhysChem* **2005**, *6*, 609–617.

(13) Hobza, P.; Havlas, Z. The fluoroform$\cdots$ethylene oxide complex exhibits a C–H$\cdots$O anti-hydrogen bond. *Chem. Phys. Lett.* **1999**, *303*, 447–452.

(14) Delanoye, S. N.; Herrebout, W. A.; Van der Veken, B. J. Improper or classical hydrogen bonding? A comparative cryosolutions infrared study of the complexes of $HCClF_2$, $HCCl_2F$, and $HCCl_3$ with dimethyl ether. *J. Am. Chem. Soc.* **2002**, *124*, 7490–7498.

(15) Qian, W.; Krimm, S. Vibrational Spectroscopy of Hydrogen Bonding: Origin of the Different Behavior of the C–H$\cdots$O Hydrogen Bond. *J. Phys. Chem. A* **2002**, *106*, 6628–6636.

(16) Qian, W.; Krimm, S. CH$\cdots$O and OH$\cdots$O hydrogen bonding in formic acid dimer structures: A QM/MM study confirms the common origin of their different spectroscopic behavior. *J. Phys. Chem. A* **2002**, *106*, 11663–11671.

(17) Mo, Y.; Wang, C.; Guan, L.; Braïda, B.; Hiberty, P. C.; Wu, W. On the nature of blueshifting hydrogen bonds. *Chem.-Eur. J.* **2014**, *20*, 8444–8452.

(18) Gu, Y.; Kar, T.; Scheiner, S. Fundamental Properties of the CH$\cdots$O Interaction: Is It a True Hydrogen Bond? *J. Am. Chem. Soc.* **1999**, *121*, 9411–9422.

(19) Li, X.; Liu, L.; Schlegel, H. B. On the physical origin of blue-shifted hydrogen bonds. *J. Am. Chem. Soc.* **2002**, *124*, 9639–9647.

(20) Hermansson, K. Blue-shifting hydrogen bonds. *J. Phys. Chem. A* **2002**, *106*, 4695–4702.

(21) Pejov, L.; Hermansson, K. On the nature of blueshifting hydrogen bonds: ab initio and density functional studies of several fluoroform complexes. *J. Chem. Phys.* **2003**, *119*, 313–324.

(22) Masunov, A.; Dannenberg, J.; Contreras, R. H. C–H Bond-Shortening upon Hydrogen Bond Formation: Influence of an Electric Field. *J. Phys. Chem. A* **2001**, *105*, 4737–4740.

(23) Alabugin, I. V.; Manoharan, M.; Peabody, S.; Weinhold, F. Electronic basis of improper hydrogen bonding: A subtle balance of hyperconjugation and rehybridization. *J. Am. Chem. Soc.* **2003**, *125*, 5973–5987.

(24) Joseph, J.; Jemmis, E. D. Red-, blue-, or no-shift in hydrogen bonds: a unified explanation. *J. Am. Chem. Soc.* **2007**, *129*, 4620–4632.

(25) Mo, Y.; Gao, J.; Peyerimhoff, S. D. Energy decomposition analysis of intermolecular interactions using a block-localized wave function approach. *J. Chem. Phys.* **2000**, *112*, 5530–5538.

(26) Mo, Y. Geometrical optimization for strictly localized structures. *J. Chem. Phys.* **2003**, *119*, 1300–1306.

(27) Mo, Y.; Bao, P.; Gao, J. Energy decomposition analysis based on a block-localized wavefunction and multistate density functional theory. *Phys. Chem. Chem. Phys.* **2011**, *13*, 6760–6775.

(28) Wang, C.; Danovich, D.; Shaik, S.; Mo, Y. A Unified Theory for the Blue-and Red-Shifting Phenomena in Hydrogen and Halogen Bonds. *J. Chem. Theory Comput.* **2017**, *13*, 1626–1637.

(29) Mao, Y.; Horn, P. R.; Head-Gordon, M. Energy decomposition analysis in an adiabatic picture. *Phys. Chem. Chem. Phys.* **2017**, *19*, 5944–5958.

(30) Khaliullin, R. Z.; Cobar, E. A.; Lochan, R. C.; Bell, A. T.; Head-Gordon, M. Unravelling the origin of intermolecular interactions using absolutely localized molecular orbitals. *J. Phys. Chem. A* **2007**, *111*, 8753–8765.

(31) Horn, P. R.; Mao, Y.; Head-Gordon, M. Probing non-covalent interactions with a second generation energy decomposition analysis using absolutely localized molecular orbitals. *Phys. Chem. Chem. Phys.* **2016**, *18*, 23067–23079.

(32) Mao, Y.; Ge, Q.; Horn, P. R.; Head-Gordon, M. On the Computational Characterization of Charge-Transfer Effects in Noncovalently Bound Molecular Complexes. *J. Chem. Theory Comput.* **2018**, *14*, 2401–2417.

(33) Ang, S. J.; Mak, A. M.; Wong, M. W. Nature of halogen bonding involving π-systems, nitroxide radicals and carbenes: a highlight of the importance of charge transfer. *Phys. Chem. Chem. Phys.* **2018**, *20*, 26463–26478.

(34) Ramos-Cordoba, E.; Lambrecht, D. S.; Head-Gordon, M. Charge-transfer and the hydrogen bond: Spectroscopic and structural implications from electronic structure calculations. *Faraday Discuss.* **2011**, *150*, 345–362.

(35) Horn, P. R.; Mao, Y.; Head-Gordon, M. Defining the contributions of permanent electrostatics, Pauli repulsion, and dispersion in density functional theory calculations of intermolecular interaction energies. *J. Chem. Phys.* **2016**, *144*, 114107.

(36) Breneman, C. M.; Wiberg, K. B. Determining atom-centered monopoles from molecular electrostatic potentials. The need for high sampling density in formamide conformational analysis. *J. Comput. Chem.* **1990**, *11*, 361–373.

(37) Shao, Y.; Gan, Z.; Epifanovsky, E.; Gilbert, A. T.; Wormit, M.; Kussmann, J.; Lange, A. W.; Behn, A.; Deng, J.; Feng, X.; Ghosh, D.; Goldey, M.; Horn, P. R.; Jacobson, L. D.; Kaliman, I.; Khaliullin, R. Z.; Kuś, T.; Landau, A.; Liu, J.; Proynov, E. I.; Rhee, Y. M.; Richard, R. M.; Rohrdanz, M. A.; Steele, R. P.; Sundstrom, E. J.; Woodcock, H. L.; Zimmerman, P. M.; Zuev, D.; Albrecht, B.; Alguire, E.; Austin, B.; Beran, G. J. O.; Bernard, Y. A.; Berquist, E.; Brandhorst, K.; Bravaya, K. B.; Brown, S. T.; Casanova, D.; Chang, C.-M.; Chen, Y.; Chien, S. H.; Closser, K. D.; Crittenden, D. L.; Diedenhofen, M.; DiStasio, R. A.; Do, H.; Dutoi, A. D.; Edgar, R. G.; Fatehi, S.; Fusti-Molnar, L.; Ghysels, A.; Golubeva-Zadorozhnaya, A.; Gomes, J.; Hanson-Heine, M. W.; Harbach, P. H.; Hauser, A. W.; Hohenstein, E. G.; Holden, Z. C.; Jagau, T.-C.; Ji, H.; Kaduk, B.; Khistyaev, K.; Kim, J.; Kim, J.; King, R. A.; Klunzinger, P.; Kosenkov, D.; Kowalczyk, T.; Krauter, C. M.; Lao, K. U.; Laurent, A.; Lawler, K. V.; Levchenko, S. V.; Lin, C. Y.; Liu, F.; Livshits, E.; Lochan, R. C.; Luenser, A.; Manohar, P.; Manzer, S. F.; Mao, S.-P.; Mardirossian, N.; Marenich, A. V.; Maurer, S. A.; Mayhall, N. J.; Neuscamman, E.; Oana, C. M.; Olivares-Amaya, R.; ONeill, D. P.; Parkhill, J. A.; Perrine, T. M.; Peverati, R.; Prociuk, A.; Rehn, D. R.; Rosta, E.; Russ, N. J.; Sharada, S. M.; Sharma, S.; Small, D. W.; Sodt, A.; Stein, T.; Stück, D.; Su, Y.-C.; Thom, A. J.; Tsuchimochi, T.; Vanovschi, V.; Vogt, L.; Vydrov, O.; Wang, T.; Watson, M. A.; Wenzel, J.; White, A.; Williams, C. F.; Yang, J.;

Yeganeh, S.; Yost, S. R.; You, Z.-Q.; Zhang, I. Y.; Zhang, X.; Zhao, Y.; Brooks, B. R.; Chan, G. K.; Chipman, D. M.; Cramer, C. J.; Goddard, W. A.; Gordon, M. S.; Hehre, W. J.; Klamt, A.; Schaefer, H. F.; Schmidt, M. W.; Sherrill, C. D.; Truhlar, D. G.; Warshel, A.; Xu, X.; Aspuru-Guzik, A.; Baer, R.; Bell, A. T.; Besley, N. A.; Chai, J.-D.; Dreuw, A.; Dunietz, B. D.; Furlani, T. R.; Gwaltney, S. R.; Hsu, C.-P.; Jung, Y.; Kong, J.; Lambrecht, D. S.; Liang, W.; Ochsenfeld, C.; Rassolov, V. A.; Slipchenko, L. V.; Subotnik, J. E.; Van Voorhis, T.; Herbert, J. M.; Krylov, A. I.; Gill, P. M.; Head-Gordon, M. Advances in molecular quantum chemistry contained in the Q-Chem 4 program package. *Mol. Phys.* **2015**, *113*, 184–215.

(38) Mardirossian, N.; Head-Gordon, M. ωB97X-V: A 10-parameter, range-separated hybrid, generalized gradient approximation density functional with nonlocal correlation, designed by a survival-of-the-fittest strategy. *Phys. Chem. Chem. Phys.* **2014**, *16*, 9904–9924.

(39) Rappoport, D.; Furche, F. Property-optimized Gaussian basis sets for molecular response calculations. *J. Chem. Phys.* **2010**, *133*, 134105.

(40) Mardirossian, N.; Head-Gordon, M. Thirty years of density functional theory in computational chemistry: an overview and extensive assessment of 200 density functionals. *Mol. Phys.* **2017**, *115*, 2315–2372.

(41) Goerigk, L.; Hansen, A.; Bauer, C. A.; Ehrlich, S.; Najibi, A.; Grimme, S. A Look at the Density Functional Theory Zoo with the Advanced GMTKN55 Database for General Main Group Thermochemistry, Kinetics and Noncovalent Interactions. *Phys. Chem. Chem. Phys.* **2017**, *19*, 32184–32215.

(42) Becke, A. D. Density-functional thermochemistry. III. The role of exact exchange. *J. Chem. Phys.* **1993**, *98*, 5648–5652.

(43) Grimme, S.; Ehrlich, S.; Goerigk, L. Effect of the damping function in dispersion corrected density functional theory. *J. Comput. Chem.* **2011**, *32*, 1456–1465.

(44) Krishnan, R.; Binkley, J. S.; Seeger, R.; Pople, J. A. Self-consistent molecular orbital methods. XX. A basis set for correlated wave functions. *J. Chem. Phys.* **1980**, *72*, 650–654.

(45) Frisch, M. J.; Pople, J. A.; Binkley, J. S. Self-consistent molecular orbital methods 25. Supplementary functions for Gaussian basis sets. *J. Chem. Phys.* **1984**, *80*, 3265–3269.

(46) Gill, P. M.; Johnson, B. G.; Pople, J. A. A standard grid for density functional calculations. *Chem. Phys. Lett.* **1993**, *209*, 506–512.

(47) Vydrov, O. A.; Van Voorhis, T. Nonlocal van der Waals density functional: The simpler the better. *J. Chem. Phys.* **2010**, *133*, 244103.

(48) Mao, Y.; Demerdash, O.; Head-Gordon, M.; Head-Gordon, T. Assessing ion-water interactions in the AMOEBA force field using energy decomposition analysis of electronic structure calculations. *J. Chem. Theory Comput.* **2016**, *12*, 5422–5437.